11

Nanocomposite PPy Coatings for Al Alloys Corrosion Protection

Kirill L. Levine

CONTENTS

11.1 Introduction

Aluminum (Al) alloys, such as Al 2024-T3, are extensively used in aircraft and construction industries because of their low density and excellent mechanical properties. Chemically pure Al is naturally protected from corrosion by an oxide layer. Al alloys are vulnerable to corrosion because they contain intermetallic impurities, such as copper, zinc, and molybdenum, whose contents can be considerably high. For example, Cu content in Al2024-T3

is close to 5%.* Impurities are distributed in alloys in a nonuniform way, resulting in the presence of clusters which become the centers for galvanic corrosion. A galvanic corrosion pair is formed between the impurity and the surrounding metal. The material that is consumed in this corrosion is usually Al as it is more reactive.

Corrosion of Al alloys results in approximately 3% annual loss of Al constructions worldwide; therefore, their corrosion protection is a serious industrial concern. This problem was recently solved by using hexavalent chromium (Cr^{6+}) coatings. Although Cr^{6+} provides satisfactory corrosion protection to Al alloys, Cr^{6+} coatings are carcinogenic. Technologies utilizing this sort of protection are therefore hazardous for human health and the environment, and currently their replacement with chromium-free alternatives has been approved in the United States and almost all other developed countries.

One of the alternatives to Cr^{6+} coatings is Mg-rich coatings [1]. The ideology of these coatings is that Mg is sacrificed for the sake of Al, thus protecting Al. These coatings have demonstrated their efficiency at a short-term run. However, their long-lasting efficiency is under question. It is not clear how these coatings will perform after all the Mg is consumed.

Among the approaches replacing Cr^{6+}, utilizing intrinsically conducting polymers (ICPs) for corrosion protection is one of the most promising.

An example of ICPs is shown in Figure 11.1. ICPs contain a double bond in the backbone of their macromolecule which is responsible for their specific properties. The property which is important for their corrosion protection performance is electroactivity. Electroactivity is the ability of a polymer film coated on an electrode to change its reduction or oxidation state under the influence of an applied potential, when the electrode is immersed in the

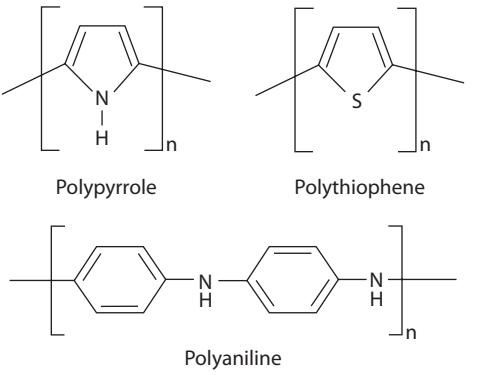

FIGURE 11.1
Example of conducting polymers.

* Composition of Al 2024-T3 (w/w %) is 3.8–4.9 Cu, 1.2–1.8 Mg, 0.50 Fe, 0.3–0.9 Mn, 0.50 Si, 0.25 Zn, 0.15 Ti, 0.1 Cr, 0.15 other unspecified elements, and Al to 100%.

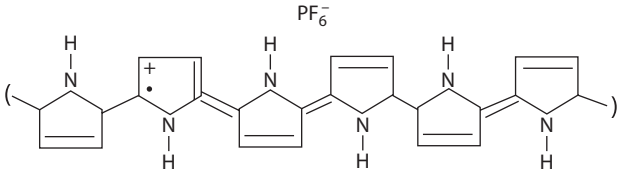

FIGURE 11.2
Example of PPy doped by a hexafluorophosphate ion.

solution of an electrolyte. Changing the reduction or oxidation state is followed by the movement of an electrolyte ion in or out of the film. This phenomenon is called "doping" and ions participating in this are referred to as "dopants." An example of a PPy film doped with PF_6^- is shown in Figure 11.2. This chapter will later discuss how ICP doping can be utilized in corrosion protection. It should be pointed out that the majority of ICPs—and PPy is not an exclusion—possess more positive oxidation potential than Al, and therefore its coating on Al surfaces possesses ennobling properties.

11.2 ICPs and Their Anticorrosion Performance

The method suggested by Kendig et al. [2] utilizes oxygen reduction inhibitors (ORIs) as dopants. ORIs, such as 2,5-dimercapto-1,3,4-thiadiazole (DMCT) (Figure 11.3), were found to significantly slow down corrosion. The mechanism of their action is shown in Figure 11.4, which can be explained by means of the following sequence:

1. As a result of corrosion, an electron was released (corrosive pit at the left).
2. An electron was absorbed by a conjugated double-bond electronic structure.
3. From the electroneutrality considerations, an ORI^- ion was released at the location of a corrosive pit (shown at the right-hand side of the figure).
4. Further corrosion was slowed down due to an ORI action.

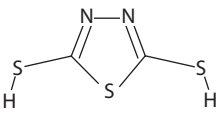

FIGURE 11.3
2,5-dimercapto 1,3,4-thiadiazole (acid form).

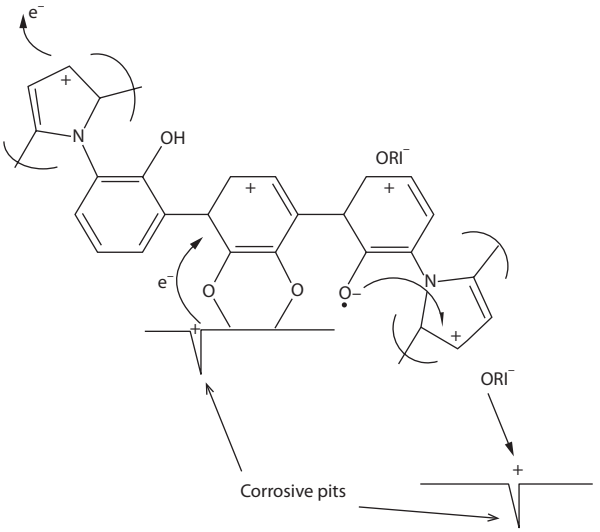

FIGURE 11.4
Schematic representation of ORI release.

Opponents of this theory have justified that this mechanism needs the corrosion to be started in order to be in force [2]. Other methods utilizing "smart" materials, such as described in the literature review [3], were suggested.

When conducting polymers are obtained on an active metal surface, they are capable of filling pores caused by imperfections in metal oxide. ICPs can form a barrier to aggressive ions which penetrate through those pores to a metal surface, therefore slowing down the corrosion [4,5].

11.3 Problems and Approaches

11.3.1 Electron Transfer Mediators and Their Application for the Deposition of Conducting Polymers

When a monomer of pyrrole or another ICP is dissolved in the solution, it can be polymerized electrochemically by a mechanism first described by Diaz [6]. But the surface of the active metal is covered with an oxide that prevents the polymer from forming an adherent uniform layer. The electrochemical method allows overcoming this difficulty with the help of so-called electron transfer mediators (ETMs). Examples of different ETMs are shown in Table 11.1. By applying positive potential to the surface of an active metal in a solution of an electrically conducting liquid containing hydroxyl ions, the surface starts to oxidize. In the presence of a monomer of a conducting

TABLE 11.1

Different Compounds with Electron Transfer Mediating Properties

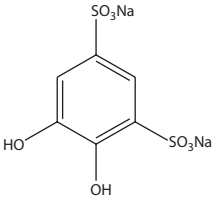	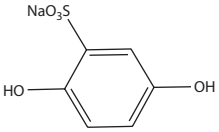	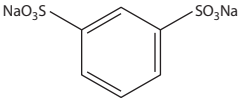
4,5-dihydroxy-1,3-benzenedisulfonate (DHBDS or Tiron)	3,6-dihydroxy-benzenesulfonate (DHBS)	1,3 dibenzenesulfonate (DBS)
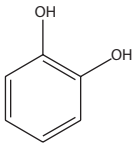		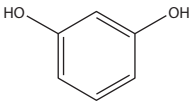
1,2 dihydroxybenzene (Catechol)	1,4 dihydroxybenzene (Hydroquinone)	1,3 dihydroxybenzene (Resorcinol)

polymer, such as pyrrole, oxidation goes more readily than polymerization and a uniform ICP layer does not form. An approach that uses ETMs allows the reduction of PPy deposition potential on Al and its alloys by nearly 500 mV, permitting ICP film deposition from an aqueous solution with high current efficiency [7–10]. A mediator whose high efficiency was shown first was disodium salt of 4,5-dihydroxy-1,3-benzenedisulfonate, (DHBDS, also known as Tiron). The mechanism of this mediator's performance is shown in Figure 11.5. When DHBDS is dissolved in an aqueous solution, it dissociates, forming anions. At the anode, their hydroxyl groups release protons and acquire positive charge, which is immediately transferred to a monomer with the proton returned back. Therefore, ETM is returned to its anionic state while the monomer is oxidized. This process repeats continuously, resulting in a collection of oxidized monomers in a pre-anodic space and their polymerization and film growth. Anions of DHBDS can also serve as dopants to ICP.

The presence of hydroxyl substitutions in a phenyl ETM phenyl ring prompted the evaluation of different compounds with hydroxyl in different positions as shown in Table 11.1.

Among those compounds, three in the top row can dissociate and serve as dopants; the three in the bottom row cannot dissociate and need additional electrolyte to make their solution electrically conductive. DBS does not have hydroxyl substitutions and was examined for comparison. In agreement with the theory of electron transfer mediation, compounds with hydroxyl substitutions in 1,2 and 1,3 positions decrease pyrrole oxidation potential most effectively. Resorcinol does not perform any mediation effect. DBS, which

FIGURE 11.5
Schematic representation of Tiron's action on pyrrole oxidation.

did not have hydroxyl substitutions, however, was also observed to decrease polymerization potential. In conclusion, in substituted benzenes, hydroxyl groups are responsible for the electron exchange between the monomer and the mediator, while sulfonate groups facilitate monomer penetration into Al oxide pores [11]. In the case where a combination of both sulfonate and hydroxyl substitutions is within the same mediator, both of the aforementioned mechanisms act simultaneously.

While designing a nanocomposite system which would slow down corrosion at the surface of active metals, issues of electron exchange have to be considered when the surface is coated by an oxide layer. The necessity to do so occurs, for example, when a "smart" response of a corroding surface is expected which results in ORI release by the schematic suggested by Kendig et al. [2], and shown in a modified way in Figure 11.4. In this figure, the reaction that provides the electron is

$$Al \rightarrow Al^{3+} + 3e^{-}$$

and the reaction that consumes the electron is

$$\tfrac{1}{2} O_2 \rightarrow O^{2-} - 2e^{-}$$

The electric driving force generated by this reaction is 1.7 V, which far exceeds PPy dedoping potential. In order to examine the process of electron transfer through an oxide layer formed in the presence of different mediators, we are interested in studying the dielectric properties of an oxide, such as the concentration of oxygen vacancies, and electrochemical potential. According to Levine et al. [12], the surface of an active metal covered by an ultrathin oxide layer was analyzed by Mott–Schottky spectroscopy.

11.3.2 Studying an Oxide Layer Formed in the Presence of Different Mediators

The fundamental property of any dielectric material is the size and structure of its bandgap, the location of energy levels introduced by donor or acceptor impurities, and Fermi level, which in the case of electrochemical equilibrium is called "electrochemical potential" [13]. The most precise electrochemical method that allows looking at the electrochemical potential is the Mott–Schottky analysis [14], in which the "electrochemical potential" for historical reasons is called the "flat band potential," and has the same meaning as Fermi level.

In order to conduct the Mott–Schottky experiment, an oxide layer was obtained in the presence of ETM by cyclic potential scanning using the procedure of the cyclic voltammetry (CV) experiment. The potential scanned from negative 1 to positive E_{max} equal to 900 mV versus Ag/AgCl, as in Ref. [10]. After

that the electrolyte was replaced by one without a mediator and the Mott–Schottky analysis was performed. The studied compounds were the benzenes with either hydroxyl, or sulfonate substitutions, or a combination of both.

The physical nature of the type of contact between an oxide film on the top of an Al and metal surface is responsible for the mechanism of electron transfer. From the microfabrication it is known that there exist three types of junction: metal-to-metal, metal-to-semiconductor (Shottky barrier), and semiconductor-to-semiconductor. As there are no specific differences between the intrinsic semiconductor and dielectric, except the size of a band-gap, it can be assumed that the oxide–Al interface possesses Shottky junction properties affected by the level of oxygen vacancies in Al oxide.

Al oxide can be described as a dielectric with an impurity comprised of oxygen vacancies (Figure 11.6).

The Mott–Schottky method is based on the determination of space charge layer capacitance C_{sc}^{-2} measured at a fixed frequency as a function of potential around an open-circuit potential (OCP)* (Figure 11.4). The Mott–Schottky relationship for a p-type semiconductor can be written as

$$C_{sc}^{-2} = -\frac{2}{\varepsilon\varepsilon_0 e N_A A^2}(E - E_{FB} - kT) \tag{11.1}$$

where

ε is the dielectric constant for Al oxide
ε_0 is the dielectric constant
e the electron charge
E is the applied potential
E_{FB} is the flat band potential
k is the Boltzmann constant

FIGURE 11.6
Zone diagram of Al oxide with the acceptor type of conductivity.

* Physical meaning of ICP is the potential of the free surface, that is, the potential of the surface which is in equilibrium with an electrolyte solution. It is characteristic to the energy which has to be spent to remove an electron from the surface, which is in some sense characteristic to corrosion.

T is the temperature
A is the sample area
N_A is the acceptor concentration

E_{FB} was found to depend on the position of hydroxyl substitutions in the benzene ring (Table 11.2). The oxide formed in the presence of the mediator with closer positions of hydroxyls possessed less electron affinity than the one formed in the presence of the mediator with larger displacement of hydroxyl groups. The oxide formed at larger E_{max} did not show this correlation (Figure 11.7). E_{max} governs the thickness of the oxide layer, and possibly the E_{FB}: barrier that electrons have to overcome to be removed from an oxide. This principle was confirmed for computerized axial tomography (CAT) and somewhat for RES; however, it did not hold for HQ, showing a correlation with the proximity of hydroxyls in the benzene ring on $E_{FB} - E_{max}$ dependence. References for electrochemical oxidative polymerization of HQ [10,15,16] and CAT [17] can be found in the literature. Summarizing, it can be said that below positive 0.6 V (below CAT and HQ polymerization potential at Al), a correlation between the position of the hydroxyl group and E_{FB} was observed.

TABLE 11.2

Flat Band Potential of Different Compounds with Only Hydroxyl Substitutions Obtained at Different E_{max}.

Compound	Position of Hydroxyl Substitutions	E_{FB}, V, versus Ag/AgCl		
		0.6	**1.2**	**1.8**
CAT	1, 2	−4.53	−4.60	−4.63
RES	1, 3	−4.60	−4.64	−4.64
HQ	1, 4	−4.63	−4.62	−4.61

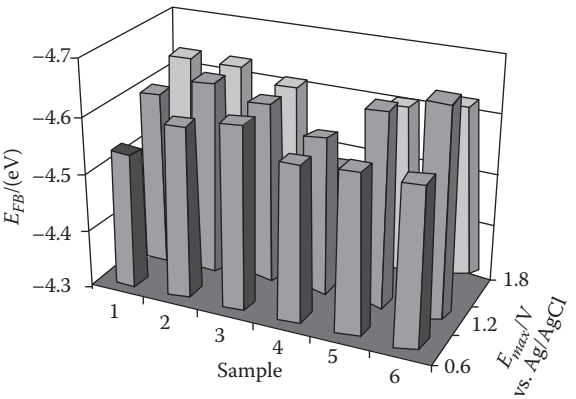

FIGURE 11.7
(See color insert.) E_{FB} of different samples as a function of potential at which oxide was obtained. 1-CAT, 2-RES, 3-HQ, 4-HQS, 5-BDS, and 6-DHBDS.

TABLE 11.3

Relative Acceptor Concentration ($N_A/N_{A\,max}$) in Oxide Obtained at 0.6 V in the Presence of Different Mediators (Normalized to CAT)

Compound	CAT	RES	HQ	HQS	BDS	DHBDS
N/N_{ACC}	1	0.602	0.679	0.270	0.292	0.138

The largest E_{FB} values were observed for DHBDS. The best corrosion protection performance of samples prepared with DHBDS was supported by monitoring experiments.

Due to the complicated structure of the Al alloy, Al oxide formed on its surface contains impurities and deviations from stoichiometry. Si^{4+} substitutions create vacancies, while Al^{2+} or Mg^{2+} generate interlattice electrons. The concentration of these charge carriers defines the type and magnitude of electrical conductivity of an oxide. Electron transfer mediators applied during the oxide deposition affect the balance between p and n defects in the Al oxide that is a p type due to oxygen vacancies. E_{FB} and impurities concentration were found to correlate with the structure of the mediator applied during the oxide deposition (Table 11.3). These data are believed to be important to understand the mechanism of electron transfer from an oxide surface to a conducting polymer which is part of a triggering device responsible for "smart" behavior.

11.3.3 PPy Deposition on Anodic Nanoporous Alumina and Anticorrosion Properties of this Coating

The rationale for depositing PPy on the oxide layer is to combine the barrier properties of Al oxide with corrosion-inhibiting properties of PPy. Chemically pure Al oxide (Al_2O_3, sometimes referred as alumina) is a dielectric and in order to deposit ICP onto an oxide of a few microns thickness, it has to be porous. In Ref. [18] Al oxide was obtained electrochemically by a method that is a simplified version of oxidation used to prepare anodic porous alumina (APA), such as described in Ref. [19]. Electrochemically, it is possible to obtain oxide in a wide range of thicknesses. The mechanism of oxide growth is described in Ref. [20]. Due to variations in the composition of the alloy, it is impossible to obtain a regular pore structure. Surface pore distribution was not regular but uniform as shown by scanning electron microscopy (SEM) (Figure 11.8). Electrochemical constant current deposition of PPy on a porous oxide (PO) surface required potentials that were sufficiently higher than the potentials necessary for PPy deposition on an Al alloy that is not oxidized (which is in fact covered by a very thin, natural oxide layer of atmospheric origination). The curve at the bottom of Figure 11.9 shows deposition of PPy onto a bare Al alloy surface in the presence of DHBDS.

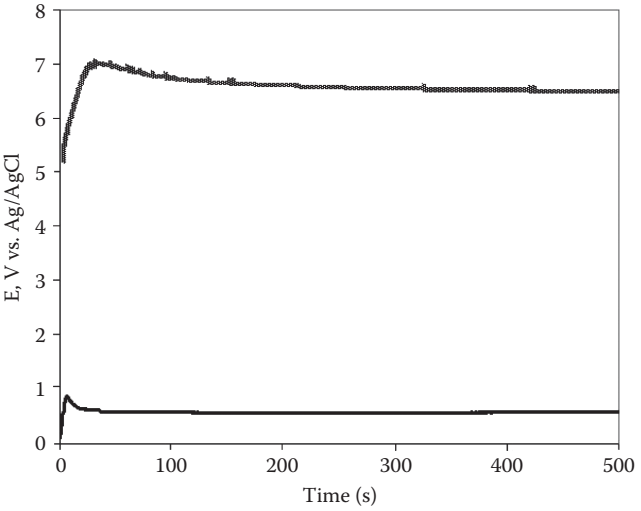

FIGURE 11.8
Galvanostatic deposition of PPy on the surface of aluminum alloy with oxide (top) and without oxide layer (bottom).

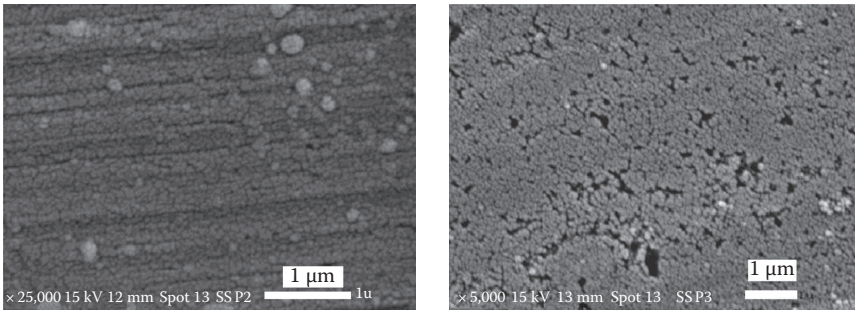

(a) (b)

FIGURE 11.9
SEM images of (a) untreated aluminum and (b) porous aluminum surface.

In this case, the deposition potential was 0.6–0.65 V*, which is a typical value for the deposition in the presence of this mediator [10]. When the Al alloy was preliminary coated with PO, the deposition started at 5.2 V, reaching approximately 7 V after the first 50 s of the experiment, followed by a slow decrease to 6.5 V. Without DHBDS, deposition on the oxide-coated

* Unless specified or table values, potentials are given versus silver/silver chloride (Ag/AgCl) reference electrode.

TABLE 11.4

OCP of Different Surfaces Determined by Potentiodynamic Experiments

Material	OCP, V vs. SCE
Bare Al control	−0.95
PPy on bare Al	−0.55
Al oxide on Al	−0.4
PPy on oxide on Al	0.0

surface was not possible (the deposition potential was above 8 V, and no PPy formation was observed). The chemical structure was identified by Fourier transform infrared spectroscopy (FTIR) as PPy in both cases with the presence of all major picks characteristic to PPy [18], suggesting that in the presence of ETM the overpotential of PPy deposition was negligible and did not result in overoxidation of a conducting polymer, which is usually observed if the potential of PPy deposition is too high [21].

Corrosion protection properties of different types of coatings were assessed by potentiodynamic (Tafel) experiments. Tafel plots allow the determination of OCP for different types of surfaces. Experiments were conducted in contact with a corrosive electrolyte, diluted Harrison solution (DHS). The results are shown in Table 11.4.

PPy on Al surface shows relatively high OCP that was shown previously by a scanning vibrating electrode technique (SVET) and reported in Ref. [22]. High thickness of Al oxide in PPy/oxide/Al structure brings OCP to the level of mercury, which is sometimes referred to as a noble metal because it can be found in some geological deposits in metallic form. Therefore, the PPy/oxide/Al structure can be considered to possess properties of noble metals.

11.3.4 Porous Structure of Oxide Film and Its Characterization by Impedance Methods

Potential drop at metal/oxide/PPy/solution interface can be formulated as

$$E_{appl} = E_{Sh} + E_{Ox} + E_{PPy\,dep} \tag{11.2}$$

where

E_{appl} is the applied potential
E_{Sh} is the potential drop due to Shottky junction
E_{ox} is the potential drop at oxide
$E_{PPy\,dep}$ is the potential drop required to for PPy deposition

The Mott–Shottky junction possesses rectifying properties; therefore, the potential drop in straight direction in a rough estimate can be neglected. Assuming that $E_{PPy\ dep}$ is the same in the presence and absence of an oxide (600 mV) and subtracting it from a steady-state potential of deposition on an oxide (6500 mV), pore resistance can be determined as 0.17 Ω from Ohms law. Potential drop at an oxide surface required for PPy deposition when the oxide was previously developed is created by the resistance of the solution inside the pores. However, taken separately, the improved mechanical contact cannot be responsible for an increased OCP; therefore, E_{Sh}, which was neglected during the calculation of the pore resistance, must be taken into consideration. The existence of this potential drop in straight direction can be seen at the volt–ampere diode curves depending on the type of electrical contact. The junction properties of the ICP–metallic interface have to be considered when surface-ennobling properties are discussed [12,23].

By calculating the area occupied by pore per unit area (approximately 3.5%) and dividing by integral pore resistance from Equation 11.1, the resistance of a single pore, assuming their connection in parallel, can be roughly estimated as 4.8 MΩ. From ultraviolet–visible (UV–VIS) interference measurements, oxide thickness was determined as 2.52 μm, assuming 5.9 V potential drop on an oxide, and field gradient along a pore was on the order of 10^6 V/m, which is enough to form PPy nucleation sites inside an oxide pore.

11.3.5 Characterization of Porous Layers by Impedance Methods

Electrical conductivity of the solution σ is contributed by the conductivity of several types of ions *i*:

$$\sigma = \sum n_i \mu_i |q_i| \tag{11.3}$$

where
- n_i is the concentration
- q_i the charge
- μ_i the mobility of *i*th ion

An oxide layer can be taken as a permeable membrane which is placed between a metal and a solution. If the membrane resistance r_{pore} is much higher than the solution resistance r_{sol} ($r_{pore} >> r_{sol}$), the measurable quantity characterizes the resistance of pores (pore resistance) [24]. The resistance of a cylindrical pore (Figure 11.10a), with index *j* ($r_{pore\ j}$), can be written as

$$r_{porej} = \rho \frac{d}{A_p} \tag{11.4}$$

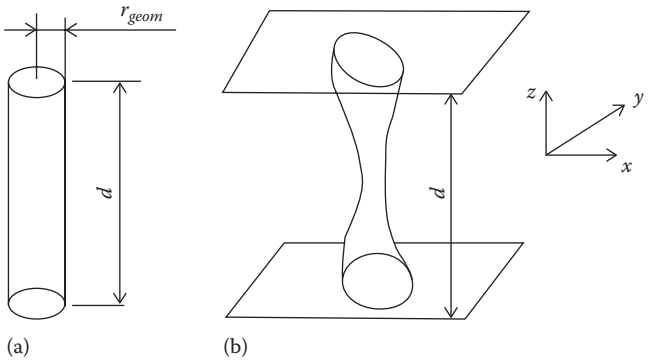

FIGURE 11.10
(a) Cylindrical and (b) noncylindrical pore.

and

$$A_p = \pi r_{geom}^2 \tag{11.5}$$

where
d is the pore length
A_p is the cross-sectional area
r_{geom} is the pore radius
ρ is the unit resistance of the solution in the pore equal to

$$\rho = \sigma^{-1} \tag{11.6}$$

If the pore is not cylindrical (Figure 11.10b), its resistance can be determined by integrating

$$r_{pore\,j} = \int_V \frac{dV}{A(x,y,z)} \tag{11.7}$$

By taking the sum of separate parallel pores by index j, the entire film resistance can be determined as

$$r_{pore}^{-1} = \sum_{j=1}^{N} r_{pore(j)}^{-1} \tag{11.8}$$

which gives a mathematical representation of pore resistance.

Measured at small frequency (1/2π Hz), the cell resistance r_{cell}, determined from Bode plot, can be written as

$$r_{cell} = r_{sol} + r_{pore} + r_{pol} \tag{11.9}$$

In this equation, r_{sol} is the solution resistance, which can be neglected, and r_{pol} is the polarization resistance, which is on the same order as r_{pore} [25]. Therefore:

$$r_{cell} \approx r_{pol} + r_{pore} \tag{11.10}$$

where r_{pol} is no more of interest because it can be eliminated by selecting zero potential, which equilibrates the film with the solution, giving

$$r_{cell} \approx r_{pore} \tag{11.11}$$

and in this case, it can be determined from the low-frequency part of the Bode plot.

In principle, the problem of determining pore size distribution from electrochemical impedance spectroscopy (EIS) data can be possibly solved. It opens possibilities of monitoring corrosion, progressive characterization of porous materials, such as fuel cell catalytic membranes, and other applications. This can be a subject for future investigation.

11.3.6 Visualizing Pore Structure by SEM Imaging

A SEM image of PPy obtained on PO (Figure 11.11a and b) shows a dense and uniform surface that is possibly a PPy-coated oxide with PPy globules on the top of the pores.

The visual appearance of the samples with PPy on an oxide surface was the same after 7 days of corrosion test as it was before the test: no delamination spots were observed, while PPy obtained by normal procedure was roughly half delaminated. Such an effect can be explained by better

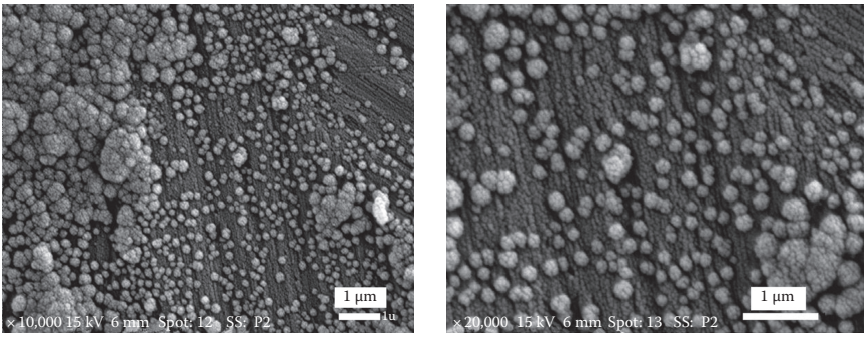

(a) (b)

FIGURE 11.11
SEM images of PPy on PO aluminum at (a) ×10,000 and (b) ×20,000 magnification. (PPy deposition: 500 s, 1 mA/cm^2, 0.1 M Py, 1 M Na_2SO_4, pH3.)

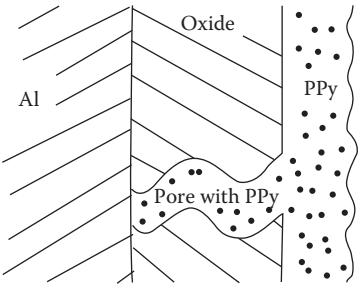

FIGURE 11.12
Schematic representation of PPy fixation on Al surface with developed Al oxide.

PPy adherence on the oxide surface because of the penetration and locking mechanism inside the pores (Figure 11.12). Adherence was responsible for the prolonged lifetime of a coating in a corroding solution. Nucleation sites for PPy deposition were formed inside the pores, while the formed PPy globules on the surface of an oxide possessed typical PPy "mushroom" morphology.

11.3.7 Smart Coatings for Corrosion Protection

In this chapter, electron kinetics has not been included as there are many publications and reviews regarding this topic in the literature [3]. However, issues related to varied porosity have not yet been discussed. If ICP concentration is high enough, ICP particles in mechanical contact with each other form the electrical percolation cluster. It was shown that there is an additional mechanism of corrosion prevention by ICP-modified nanoparticles: the nanoparticles in mechanical contact with each other provide passes for aggressive ions to penetrate into the coating [26], thus enhancing corrosion. Consequently, approaches where ICP concentration is below the mechanical percolation level are now of interest. When ICP concentration is decreased, it is still possible for electrons to move within the coating by a hopping or tunneling mechanism (such as variable range hopping [VRH] between clusters of variable size [27] or fluctuation-induced tunneling [28]). Ionic movement is not strongly affected by ICP.

While electrons hop or tunnel between nanoparticles, ions penetrate through the coating by diffusion. Without any fillers or inhomogeneities, there is only uniform diffusion [29]: penetration of ions and moisture into the coating through intermolecular spaces. In the presence of additives, such as nanoparticles or nanoflakes (Figure 11.13), uniform diffusion (Figure 11.14a) is interrupted (Figure 11.14b). However, nanoadditives introduce the mechanism of nonuniform diffusion.

ICP undoping caused changing volume, which was experimentally confirmed [30–33]. A volume increase of 8% during undoping was shown for

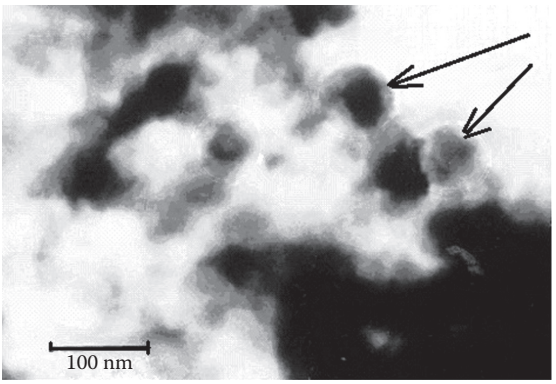

FIGURE 11.13
TEM image of nanoparticle modified with PPy (shown by arrows). (From Tallman, D.E. et al., *Appl. Surf. Sci.*, 254, 5452, 2008.)

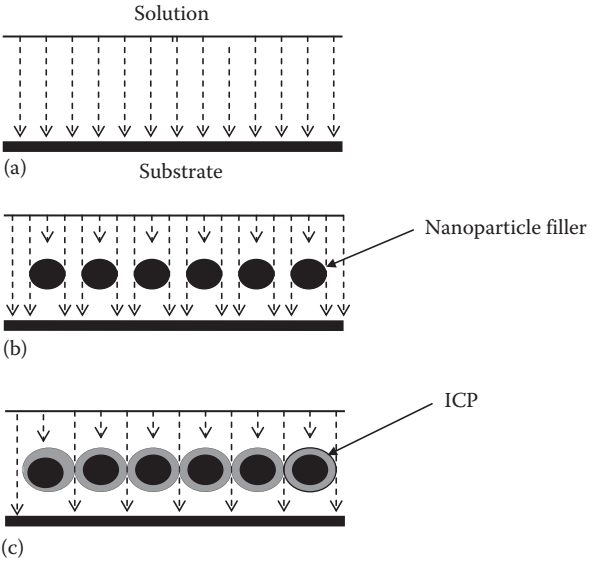

FIGURE 11.14
Schematic representation of diffusion into the coating: (a) Coating without filler. (b) Diffusion through coating with PPy-modified nanoparticle filler. (c) PPy-modified nanoparticles swelling under the influence of an electrolyte.

poly(3-octyl-thiophene) gel [31], and 12.5% volume increase for PPy doped with polystyrene sulphonate [32]. A similar effect was discovered for PPy doped with perchlorate ions [33]. The application of this effect in corrosion protection is shown schematically in Figure 11.14c. During swelling, PPy absorbed additional moisture that penetrated inside the coating through the

voids [34]. Levine et al. [34] suggested that swelling of PPy-filled voids blocks passes for ion permeation inside the coating (Figure 11.14c). Experimental confirmation of this finding was provided by EIS.

EIS is a technique in which alternating frequency potential is applied to study the system and current response is recorded [35]. EIS data are displayed with the help of the Nyquist plot, which is the imaginary part of impedance versus the real part, and the Bode plot, which is the real part of the impedance versus frequency. EIS data revealed two phases of a coating containing a nanoparticle filler (Figure 11.15). Phase I, associated with high capacitance, was related to the nanoparticle filler, while phase II, associated with low capacitance, was due to the continuous phase of the coating [4]. While phase I changed its shape and size due to swelling, phase II remained relatively intact.

From the Bode plot it was established that phase I changed its charge transfer resistance from 53 to 22.5 KΩ when nanoparticle contents decreased from 2.0% to 0.5%. The high-frequency semicircle resembles the same pattern regardless of the amount of nanoparticle filler with charge transfer resistance within the range of 9.5–12.5 KΩ. After immersion, samples with

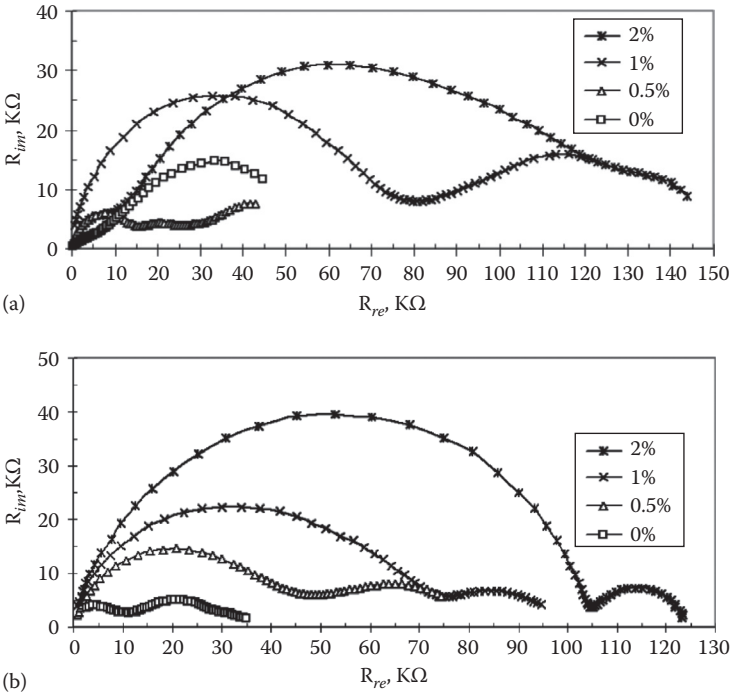

FIGURE 11.15
Nyquist plots for samples after (a) 24 and (b) 168 h of corrosion test. "Large" semicircles starting from the origin (high-frequency phase), and "small" semicircles on the right (low-frequency phase) responsible for diffusion. Percentages show nanoparticle contents.

the nanoparticle filler increased their impedance, which is usually related to the barrier property, which was attributed to the swelling of PPy-modified nanoparticles that blocked the passes to aggressive ions through the coating.

11.4 Conclusions

In this study, some aspects of corrosion protection methods and approaches related to intrinsically conducting polymers, such as polypyrrole, and active metals, such as aluminum were summarized. This study, however, did not intend to cover the entire problem in its fundamental meaning; it was focused on aspects of diffusion-linked smart behavior with relation to oxide properties that seemed important to us. Two models were discussed and the correlation between them was shown: surface ennobling by ICP, slowing down corrosion, and clogging pores by swelled ICP, thus blocking passes to aggressive ions. In practically applied anticorrosion coatings, these processes are carried out simultaneously. EIS was reviewed as a suitable method for taking a close look at diffusion through pores of variable size. The creation of new anticorrosion smart materials was also discussed.

Acknowledgments

The author acknowledges Dr. Dennis E. Tallman from North Dakota State University for his guidance throughout a significant part of this project and Dr. Valery V. Malev from St. Petersburg State University for valuable discussions.

References

1. D. Battocchi, A. M. Simões, D. E. Tallman, and G. P. Bierwagen, *Corros. Sci.*, 2006, 48(5), 1292–1306.
2. M. Kendig, M. Hon, and L. Warren, *Prog. Organ. Coat.*, 2003, 47, 183–189.
3. K. B. Kashi and V. J. Gelling, *Smart Nanocompos.*, 2(1), 55–83.
4. D. E. Tallman, K. L. Levine, C. Siripirom, V. J. Gelling, J. P. Bierwagen, and S.G. Croll, *Appl. Surf. Sci.*, 2008, 254, 5452–5459.
5. K. L. Levine, V. Fen, N. N. Nikonorova, V. M. Svetlichnyi, V. E. Yudin, L. A. Myagkova, and N. S. Pshchelko, *Smart Nanocompos.*, 3(1), 49–58.

6. T. A. Scotheim, (ed.), *Handbook of Conducting Polymers*, 1st edn., 1983. Marcel Dekker, New York.
7. D. E. Tallman, C. Vang, G. G. Wallace, and G. P. Bienragen, *J. Electrochem. Soc*., 2002, 149, 173.
8. D. E. Tallman, M. P. Dewald, C. K. Vang, G. G. Wallace, and G. P. Bierwagen. *Curr. Appl. Phys*., 2004, 4, 137.
9. D. E. Tallman, C. K. Vang, M. P. Dewald, G. G. Wallace, and G. P. Bierwagen, *Synth. Met*., 2003, 135–136, 33.
10. K. L. Levine, D. E. Tallman, and G. P. Bierwagen, *Aust. J. Chem.*, 2005, 58(4), 294–301.
11. K. Naoi, M. Takeda, H. Kanno, M. Sakakura, and A. Shimada, *Electrochim. Acta*, 2000, 45(20), 3413–3421.
12. K. L. Levine, D. E. Tallman, and G. P. Bierwagen, *J. Mater. Process. Technol*., 2008, 199, 321–326.
13. L. I. Antropov, *Theoretical Electrochemistry*, Mir Publishers, Moscow, Russia, (1978).
14. N. F. Mott, *Proc. Roy. Soc*., 1939, A 171, 27.
15. J. S. Foos and S. M. Erker, *J. Electrochem. Soc*., 1986, 133, 836.
16. K. Yamamoto, T. Asada, and K. Nishide, *Bull. Chem. Soc. Jpn*., 1990, 63, 1211.
17. J. Davis, D. H. Vaughan, and M. F. Cardosi, *Electrochim. Acta*, 1997, 43(3–4), 291–300.
18. K. L. Levine, D. E. Tallman, and G. P. Bierwagen, *ECS Transactions*, 2005, 1(4), 81–91.
19. Y. Zhao, M. Chen, Y. Zhang, T. Xu, and W. Liu, *Mater. Lett*., 2005, 59(1), 40–43.
20. M. M. Lorengel, *Mater. Sci. Eng*., 1993, R11, 243–294.
21. I. Rodriguez, B. R. Scharifker, and J. Mostany, *J. Electroanal. Chem*. 2000, 491(1–2), 117–125.
22. J. He, D. E. Tallman, and G. P. Bierwagen, *J. Electrochem. Soc*., 2004, 151(12), B644–B651.
23. B. Wessling, *Mater. Corros*., 1996, 47, 439.
24. K. L. Levine and J. O. Iroh, *J. Porous Mater*., 2004, 11, 87–95.
25. K. L. Levine and N. S. Pshchelko, *Polym. Sci. Series A (Polymer Physics)*, 2011, 53(6), 510–520.
26. M. Rohwerder and A. Michalik, *Electrochim. Acta*, 2007, 53, 1300–1313.
27. N. F. Mott and E. A. Davis, *Electronic Properties in Non-Crystalline Materials*, 1971. Clarendon press, Oxford, New York.
28. P. Sheng, *Phys. Rev. B*, 1980, 21, 2180.
29. E. L. Cussler, *J. Membr. Sci*., 1990, 52(3), 275–288.
30. T. Okamoto, Y. Kato, K. Tada, and M. Onoda, *Thin Solid Films*, 2001, 393(1–2), 383–387.
31. X. Chen and O. Inganas, *Synth. Met*., 1995, 74, 159–164.
32. M. F. Suarez and R. G. Compton, *J. Electroanal. Chem*., 1999, 462(2), 211–221.
33. M. Pyo and C.-H. Kwak, *Synth. Met*., 2005, 150, 133–137.
34. K. L. Levine, D. E. Tallman, and G. P. Bierwagen, *5th International Symposium "Molecular order and Mobility*," Publication in meeting proceedings, St. Petersburg, Russia, June 20, 2005.
35. A. J. Bard and L. R. Faulkner, *Electrochemical Methods; Fundamentals and Applications*, 2000. Wiley Interscience Publications, New York.